New Astronomy 14 (2009) 277–284

Contents lists available at ScienceDirect

New Astronomy

journal homepage: www.elsevier.com/locate/newast

Time damping of non-adiabatic MHD slow and thermal waves in a prominence medium: Effect of a background flow

M. Carbonell [a], R. Oliver [b], J.L. Ballester [b,*]

[a] Departament de Matemàtiques i Informàtica, Universitat de les Illes Balears, E-07122, Palma de Mallorca, Spain
[b] Departament de Física, Universitat de les Illes Balears, E-07122, Palma de Mallorca, Spain

ARTICLE INFO

Article history:
Received 15 July 2008
Received in revised form 21 August 2008
Accepted 3 September 2008
Available online 10 September 2008
Communicated by W. Soon

PACS:
96.60.–j
96.60.P–

Keywords:
Sun: oscillations
Sun: magnetic fields
Sun: corona
Sun: prominences

ABSTRACT

Material flows are typical features of prominences and are routinely observed in Hα, UV and EUV lines. Therefore, including a magnetic field-aligned background flow, we study the effect of flows on the damping of non-adiabatic magnetohydrodynamic (MHD) waves in a magnetised unbounded prominence medium, and we explore the observational implications. We have linearised the non-adiabatic MHD equations and, considering only field-aligned propagation, we focus our study in the behaviour of thermal and slow waves. When a flow with a constant speed is present, two slow waves, with different periods, appear, while the damping time remains unchanged. On the other hand, the thermal wave becomes in this case a propagating wave, with finite period, while its damping time remains also unmodified. As a consequence of the changes in the periods produced by the flow, the damping per period of the different waves is modified. In the case of slow waves, and for a fixed flow speed, the damping per period of the high-period slow wave is increased while the opposite happens for the low-period slow wave, and the strongest finite damping per period, for the high-period slow wave, is obtained for flow speeds close to the non-adiabatic sound speed. In the case of the thermal wave, a finite value for the damping per period is obtained for any non-zero flow speed, and in this case the strongest finite damping per period is obtained for values of the flow speed close to zero. Furthermore, we point out that there is the possibility to have slow and thermal waves having the same period, the same damping time, or both simultaneously, which makes the proper identification of the waves for an external observer extremely difficult. Then, if flows are ubiquitous in prominences the observational determinations of periods and damping per period, made by an external observer, include its effect, and for a proper identification, information about the wavelength, flow speed and perturbations should be needed, which constitutes a truly difficult observational task.

1. Introduction

Flows seem to be an ubiquitous feature in prominences and filaments and are routinely observed in Hα, UV and EUV lines. In Hα quiescent filaments typical velocities between 5 and 20 km/s are found (Zirker et al., 1998; Lin et al., 2003, 2007) and, due to physical conditions in prominence plasma, they seem to be field-aligned. Higher velocities have been also reported in the case of active filaments. Another interesting feature observed in filament flows is counterstreaming, which consists in simultaneous flowing in opposite directions within closely spaced adjacent threads (Zirker et al., 1998).

On the other hand, the presence of small-amplitude oscillations in quiescent prominences has been widely reported (Ballester, 2006; Banerjee et al., 2007) and, up to now, only the time damping of these oscillations has been determined unambiguously from observations. Reliable values for the damping time, τ_D, have been derived, from different Doppler velocity time series, by Molowny-Horas et al. (1999) and Terradas et al. (2002), in prominences, and by Lin (2004), in filaments. The values of τ_D thus obtained are usually between 1 and 4 times the corresponding period, and large regions of the prominence/filament display similar damping times. Furthermore, some determinations about the wavelengths of the MHD waves, probably responsible for prominences/filament oscillations, have been obtained. For instance, Molowny-Horas et al. (1997) determined a maximum value of 20,000 km, while Terradas et al. (2002) obtained values of 67,500, 50,000 and 44,000 km. Also, Lin et al. (2007) have determined the wavelength of oscillations in filament threads obtaining a value of about 3000 km.

Small-amplitude oscillations in quiescent prominences have been interpreted in terms of MHD waves (Oliver and Ballester,

* Corresponding author. Fax: +34 941173426.
E-mail addresses: marc.carbonell@uib.es (M. Carbonell), ramon.oliver@uib.es (R. Oliver), joseluis.ballester@uib.es (J.L. Ballester).

1384-1076/$ - see front matter © 2008 Elsevier B.V. All rights reserved.
doi:10.1016/j.newast.2008.09.001

2002; Ballester, 2006) and explanations for the time damping of prominence oscillations based on linear non-adiabatic MHD waves have been proposed (Carbonell et al., 2004; Terradas et al., 2001, 2005; Soler et al., 2007).

Taking into account the presence of flows and time damped oscillations in prominences/filaments, our main aim here is to include a background flow in the prominence medium and to explore the theoretical and observational effects produced by its presence on the time damping of non-adiabatic MHD waves. The layout of the paper is as follows: in Section 2, the equilibrium model and some theoretical considerations are presented; in Section 3, the main results are discussed; finally, in Section 4, conclusions are drawn.

2. Basic equations and theoretical considerations

2.1. Linearised equations

As a background model, we use a homogeneous unbounded medium threaded by a uniform magnetic field along the x-direction, and with a field-aligned background flow. The equilibrium magnitudes of the medium are given by

$$p_0 = \text{const.}, \quad \rho_0 = \text{const.}, \quad T_0 = \text{const.},$$
$$\mathbf{B_0} = B_0\hat{e}_x, \quad \mathbf{v}_0 = v_0\hat{e}_x,$$

with B_0 = constant and v_0 = constant. The effect of gravity has been ignored and the basic MHD equations for the discussion of non-adiabatic MHD waves are:

$$\frac{\mathrm{D}\rho}{\mathrm{D}t} + \rho\nabla\cdot v = 0, \tag{1}$$
$$\rho\frac{\mathrm{D}\mathbf{v}}{\mathrm{D}t} = -\nabla p + \frac{1}{\mu}(\nabla\times\mathbf{B})\times\mathbf{B} + \rho g, \tag{2}$$
$$\rho T\frac{\mathrm{D}s}{\mathrm{D}t} + \rho L(\rho,T) - \nabla\cdot(\kappa\cdot\nabla T) = 0, \tag{3}$$
$$\frac{\partial\mathbf{B}}{\partial t} = \nabla\times(\mathbf{v}\times\mathbf{B}), \tag{4}$$
$$\nabla\cdot\mathbf{B} = 0, \tag{5}$$
$$p = \frac{\rho RT}{\tilde{\mu}}, \tag{6}$$

where $\frac{\mathrm{D}}{\mathrm{D}t} = \frac{\partial}{\partial t} + \mathbf{v}\cdot\nabla$ is the material derivative for time variations following the motion. In Eq. (3), the term $\nabla\cdot(\kappa\cdot\nabla T)$ represents the thermal conduction, although in our case perpendicular thermal conduction has been neglected, and L is the heat-loss function which depends on the local plasma parameters. In the case of an equilibrium with uniform temperature, such as we consider here, the heat-loss function is

$$L(\rho_0, T_0) = 0.$$

Usually, in solar applications this function represents the difference between an arbitrary heat input and a radiative loss function which, in our case, has been chosen as the optically thin radiative loss function (Hildner, 1974). Then, our heat-loss function is given by

$$L(\rho,T) = \chi^*\rho T^{\alpha} - h\rho^{\mathrm{a}}T^{b}, \tag{7}$$

χ^* and α being piecewise functions depending on the temperature (Hildner, 1974). The use of an optically thin plasma radiative cooling seems to be a reasonable approach for coronal, or almost coronal, conditions, while it may not be valid for prominence conditions because they are optically thick. In this case, the radiative losses from the internal part of the prominence are greatly reduced and this can be represented by changing the exponent α in the cooling function, for temperatures $T \leqslant 10^4$ K, from $\alpha = 7.4$ to 17.4 (Milne et al., 1979) or $\alpha = 30$ (Rosner et al., 1978), as well as by changing χ^* accordingly (Carbonell et al., 2004). Finally, the last term in Eq. (7) represents an arbitrary heating function which can be modified by taking different values for the exponents a and b. In our case, different heating scenarios have been considered, and the values taken into account for exponents a and b in Eq. (7) are (Rosner et al., 1978; Dahlburg and Mariska, 1988)

(1) Constant heating per unit volume ($a = b = 0$).
(2) Constant heating per unit mass ($a = 1, b = 0$).
(3) Heating by coronal current disipation ($a = 1, b = 1$).
(4) Heating by Alfvén mode/mode conversion ($a = b = 7/6$).
(5) Heating by Alfvén mode/anomalous conduction damping ($a = 1/2, b = -1/2$).

Considering small perturbations from the equilibrium in the form

$$\mathbf{B}(t,\mathbf{r}) = \mathbf{B}_0 + \mathbf{B}_1(t,\mathbf{r}), \quad p(t,\mathbf{r}) = p_0 + p_1(t,\mathbf{r}),$$
$$\rho(t,\mathbf{r}) = \rho_0 + \rho_1(t,\mathbf{r}), \quad T(t,\mathbf{r}) = T_0 + T_1(t,\mathbf{r}),$$
$$\mathbf{v}(t,\mathbf{r}) = \mathbf{v}_0 + \mathbf{v_1}(t,\mathbf{r}),$$

we linearise the basic equations (1)–(6) to obtain

$$\left(\frac{\partial}{\partial t} + \mathbf{v}_0\cdot\nabla\right)\rho_1 + \rho_0\nabla\cdot\mathbf{v}_1 = 0, \tag{8}$$

$$\rho_0\left(\frac{\partial}{\partial t} + \mathbf{v}_0\cdot\nabla\right)\mathbf{v}_1 = -\nabla p_1 + \frac{1}{\mu}(\mathbf{B}_0\cdot\nabla)\mathbf{B}_1 - \frac{1}{\mu}\nabla(\mathbf{B}_0\cdot\mathbf{B}_1), \tag{9}$$

$$\left(\frac{\partial}{\partial t} + \mathbf{v}_0\cdot\nabla\right)(p_1 - c_s^2\rho_1) = (\gamma-1)(\mathbf{B}_0\cdot\nabla)\left[\frac{\kappa_\parallel}{B_0^2}(\mathbf{B}_0\cdot\nabla)T_1\right] - (\gamma-1)\rho_0(L_\rho\rho_1 + L_T T_1), \tag{10}$$

$$\left(\frac{\partial}{\partial t} + \mathbf{v}_0\cdot\nabla\right)\mathbf{B}_1 = \nabla\times(\mathbf{v}_1\times\mathbf{B}_0), \tag{11}$$
$$\nabla\cdot\mathbf{B}_1 = 0, \tag{12}$$
$$\frac{p_1}{p_0} - \frac{\rho_1}{\rho_0} - \frac{T_1}{T_0} = 0, \tag{13}$$

where $\kappa_\parallel = 10^{-11}T^{5/2}$, and $c_s^2 = \frac{\gamma p_0}{\rho_0}$, is the adiabatic sound speed squared. In the above linearised equations, the important difference with respect to the non-adiabatic case without flow is the operator $\frac{\partial}{\partial t} + \mathbf{v}_0\cdot\nabla$ (Goedbloed and Poedts, 2004). Since the medium is unbounded we can perform a Fourier analysis in plane waves and assume perturbations behaving like $\mathrm{e}^{\mathrm{i}(\omega t - \mathbf{k}\cdot\mathbf{r})}$, and with no loss of generality we choose the z-axis so that the wavevector $\mathbf{k}$ lies in the xz-plane, so that

$$\mathbf{k} = k_x\hat{\mathbf{e}}_x + k_z\hat{\mathbf{e}}_z.$$

Then, the above operator becomes $\mathrm{i}(\omega - k_x v_0)$, which points out that in the presence of a background flow the frequency suffers a Doppler shift given by $k_x v_0$ and that the wave frequency, ω, for the non-adiabatic case with flow can be obtained from

$$\omega = \Omega + k_x v_0, \tag{14}$$

Ω being the wave frequency for the non-adiabatic case without flow. On the other hand, these frequencies can be described in a different manner, Ω corresponds to the frequency measured by an observer linked to the flow rest frame, while ω would correspond to the frequency measured by an observer linked to an external inertial rest frame.

Then, the following scalar equations are obtained:

$$\Omega\rho_1 - \rho_0(k_x v_x + k_z v_z) = 0, \tag{15}$$
$$\Omega\rho_0 v_x - k_x p_1 = 0, \tag{16}$$

$$\Omega\rho_0 v_y + \frac{1}{\mu}B_{0x}k_x B_{1y} = 0, \tag{17}$$

$$\Omega\rho_0 v_z - k_z p_1 + \frac{1}{\mu}B_{0x}(k_x B_{1z} - k_z B_{1x}) = 0, \tag{18}$$

$$\Omega B_{1x} - B_{0x}k_z v_z = 0, \tag{19}$$

$$\Omega B_{1y} + B_{0x}k_x v_y = 0, \tag{20}$$

$$\Omega B_{1z} + B_{0x}k_x v_z = 0, \tag{21}$$

$$\frac{p_1}{p_0} - \frac{\rho_1}{\rho_0} - \frac{T_1}{T_0} = 0, \tag{22}$$

$$\mathrm{i}\Omega p_1 - \mathrm{i}\Omega c_s^2\rho_1 + (\gamma-1)(\kappa_\parallel k_x^2 + \rho_0 L_T)T_1 + (\gamma-1)(L+\rho_0 L_\rho)\rho_1 = 0. \tag{23}$$

Eqs. (17) and (20) are decoupled from the rest and describe Alfvén waves. The frequency, ω, of the Alfvén waves detected by an observer external to the flow is also Doppler shifted and is given by

$$\omega = k_x(v_0 \pm c_a),$$

where $c_a = \sqrt{\frac{B_{0x}^2}{\mu\rho_0}}$ is the Alfvén velocity. However, since Alfvén waves are not damped by thermal effects they are not investigated here. Next, we have eliminated the perturbations p_1, T_1, ρ_1, B_{1x}, B_{1z} in favour of v_x, v_z, thus obtaining two algebraic equations for the velocity perturbations. Then, imposing that the determinant of this algebraic system be zero, factoring out the expression $-B_0^2k_x^2 + \mu\Omega^2\rho_0$, and taking $k_x = k\cos\theta$ and $k_z = k\sin\theta$, the resulting dispersion relation can be written as

$$\Omega^5 - \frac{\mathrm{i}AT_0}{p_0}\Omega^4 - k^2(c_a^2+c_s^2)\Omega^3 + \mathrm{i}k^2\left(\frac{AT_0c_a^2}{p_0} + \frac{AT_0 - H\rho_0}{\rho_0}\right)\Omega^2 + c_a^2c_s^2k^4\cos^2\theta\Omega + \frac{\mathrm{i}c_a^2k^4(H\rho_0 - AT_0)\cos^2\theta}{\rho_0} = 0 \tag{24}$$

with

$$A = (\gamma-1)\kappa_\parallel k_x^2 + (\gamma-1)\rho_0 L_T, \tag{25}$$

$$H = (\gamma-1)(L+\rho_0 L_\rho). \tag{26}$$

In both expressions, the factors L_ρ, L_T are

$$L_\rho = \left(\frac{\partial L}{\partial\rho}\right)_T$$

and

$$L_T = \left(\frac{\partial L}{\partial T}\right)_p,$$

with T and p held constant, respectively, at the equilibrium state.

2.2. The behaviour of the non-adiabatic sound speed

From Eq. (10) the density and pressure perturbations can be related using a non-adiabatic sound speed, Λ, instead of the adiabatic sound speed c_s. The complex non-adiabatic sound speed, $\Lambda = \Lambda_R + \mathrm{i}\Lambda_I$, is given by

$$\Lambda = \left\{\frac{c_s^2}{\gamma}\left[\frac{(\gamma-1)\left(\frac{T_0}{p_0}\kappa_\parallel k_x^2 + \omega_T - \omega_\rho\right) + \mathrm{i}\gamma\Omega}{(\gamma-1)\left(\frac{T_0}{p_0}\kappa_\parallel k_x^2 + \omega_T\right) + \mathrm{i}\Omega}\right]\right\}^{0.5}, \tag{27}$$

with $\omega_\rho = \frac{\rho_0}{p_0}(L+\rho_0 L_\rho)$, $\omega_T = \frac{\rho_0}{p_0}L_T T_0$ (Soler et al., 2007).

From Eq. (27), we know that the non-adiabatic sound speed depends on the physical conditions of the medium, the horizontal wavenumber and the frequency. Then, keeping the same physical conditions, when the wavenumber is modified the frequency is also modified, and the numerical value of the real part of the non-adiabatic sound speed changes. In order to perform meaningful comparisons between theory and observations, we have taken into account the few observational determinations of wavelengths (Molowny-Horas et al., 1997; Terradas et al., 2002; Lin et al., 2007) made up to now. The behaviour of Λ_R versus k_x, for different prominence regimes (Carbonell et al., 2004), can be seen in Fig. 1, in which we have shaded the interval of wavenumbers between 10^{-8}–10^{-6} m^{-1}, which corresponds to the range of observationally determined wavelengths, between 10^5 km and 5×10^3 km. This figure points out that for wavenumbers equal or smaller than 10^{-4} m^{-1} there are differences between the non-adiabatic sound speeds of the different prominence regimes. The behaviour of Λ_R versus k_x shown in Fig. 1 can be easily understood with the help of Fig. 2. For horizontal wavenumbers between 10^{-10} m^{-1} and 10^{-5} m^{-1}, the perturbed heat-loss terms in the linearised energy equation (Eq. (23)) are responsible for the time damping of oscillations; for horizontal wavenumbers between 10^{-5} m^{-1} and 10^{-2} m^{-1} the effect of neglecting heating and radiation or neglecting thermal conduction is similar since in this interval both curves are overplotted and the numerical value of Λ_R becomes almost equal to the numerical value of the adiabatic sound speed c_s; next, for horizontal wavenumbers between 10^{-2} m^{-1} and 1 m^{-1}, the time damping is dominated by the perturbed thermal conduction term in the linearised energy equation (Eq. (23)); finally, for wavenumbers greater than 1 m^{-1}, the isothermal regime is attained and the value of Λ_R corresponds to the isothermal sound speed.

When adiabatic magnetoacoustic waves are considered with $c_s < c_a$ and $\theta = 0$, the frequencies, ω^a, for the fast and slow adiabatic waves are given by $\omega^a_{fast} = \pm k_x c_a$ and $\omega^a_{slow} = \pm k_x c_s$ giving place to two slow and fast magnetoacoustic waves propagating in opposite directions. When a background flow with speed v_0 is added to the previous situation, the frequencies become $\omega^{a'}_{fast} = k_x(v_0 \pm c_a)$ and $\omega^{a'}_{slow} = k_x(v_0 \pm c_s)$, so, we obtain two slow waves, with frequencies $\omega^{a'}$ measured by an external observer, higher and lower than in the static case, and the same happens for fast waves. When $\mathbf{v_0}$ and $\mathbf{B}_0$ point in the same direction and $v_0 > c_s, c_a$, the two slow and fast waves propagate in the same direction as the flow. When $c_s < v_0 < c_a$, we have two slow waves propagating in the flow direction while the fast waves propagate in opposite directions and, finally, when $v_0 < c_s, c_a$ we have two slow and fast waves propagating in opposite directions.

From the dispersion relation (24) we obtain one purely imaginary frequency, corresponding to the thermal wave, while the rest of the frequencies consist of two pairs: one pair represents the slow mode, whereas the other represents the fast mode. For each pair (Ω_1, Ω_2), $\Omega_1 = \Omega_R + \mathrm{i}\Omega_I$ and $\Omega_2 = -\Omega_R + \mathrm{i}\Omega_I$ (Carbonell et al., 2004). Then, for comparison with the adiabatic case, we expect

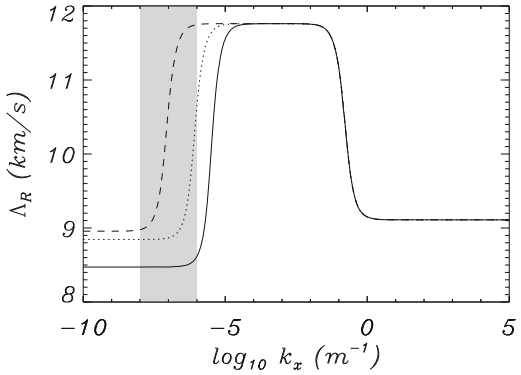

Fig. 1. Real part of the non-adiabatic sound speed, Λ_R, versus the wavenumber, k_x, for prominence regimes 1.1 (continuous line), 1.2 (dotted line) and 1.3 (dashed line). The shaded region indicates the interval of observed wavelengths. A constant heating per unit volume $a = b = 0$ has been considered and the flow speed is $v_0 = 15$ km/s.

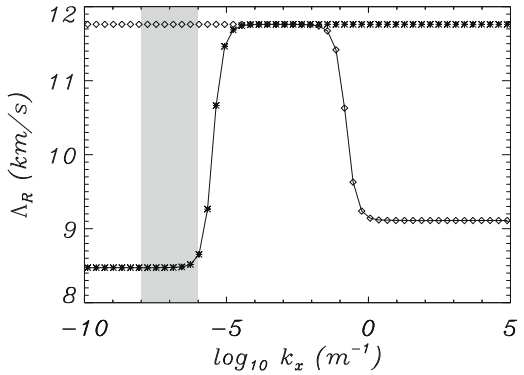

Fig. 2. Real part of the non-adiabatic sound speed, Λ_R, versus the wavenumber, k_x. General case including heating, radiation and thermal conduction (continuous line); case including heating, radiation and a negligible thermal conduction (asterisks); case including only thermal conduction (diamonds). The shaded region indicates the interval of observed wavelengths. The physical conditions correspond to prominence regime 1.1 with a constant heating per unit volume $a = b = 0$. The flow speed is $v_0 = 15$ km/s.

that in the non-adiabatic case the frequencies for slow and fast waves must be expressed as $\Omega = \pm k_x \Lambda$ and $\Omega = \pm k_x c_a$, respectively. Then, if we consider a background flow in the non-adiabatic case we obtain two fast waves with frequencies, measured by an external observer, given by $\omega_{fast} = k_x(v_0 \pm c_a) + i\omega_{Ifast}$, two slow waves with frequencies, $\omega_{slow} = k_x(v_0 \pm \Lambda_R) + i\omega_{Islow}$, and a thermal wave having now a complex frequency. Then, two interesting features appear: (a) From Eq. (14) it becomes evident that the effect of the flow is to modify the real part of the frequency, while the imaginary part remains unchanged, which will have a direct effect on the damping per period of MHD waves; (b) the thermal wave, which was not propagating in the non-adiabatic case without flow since the frequency was purely imaginary, becomes now a propagating one, with the real part of the frequency given by $\omega = k_x v_0$, while the imaginary part remains unchanged. Then, a finite damping per period can be obtained for the thermal wave.

3. Results

Carbonell et al. (2004) pointed out that fast waves are almost undamped by thermal mechanisms, then, in this study we have

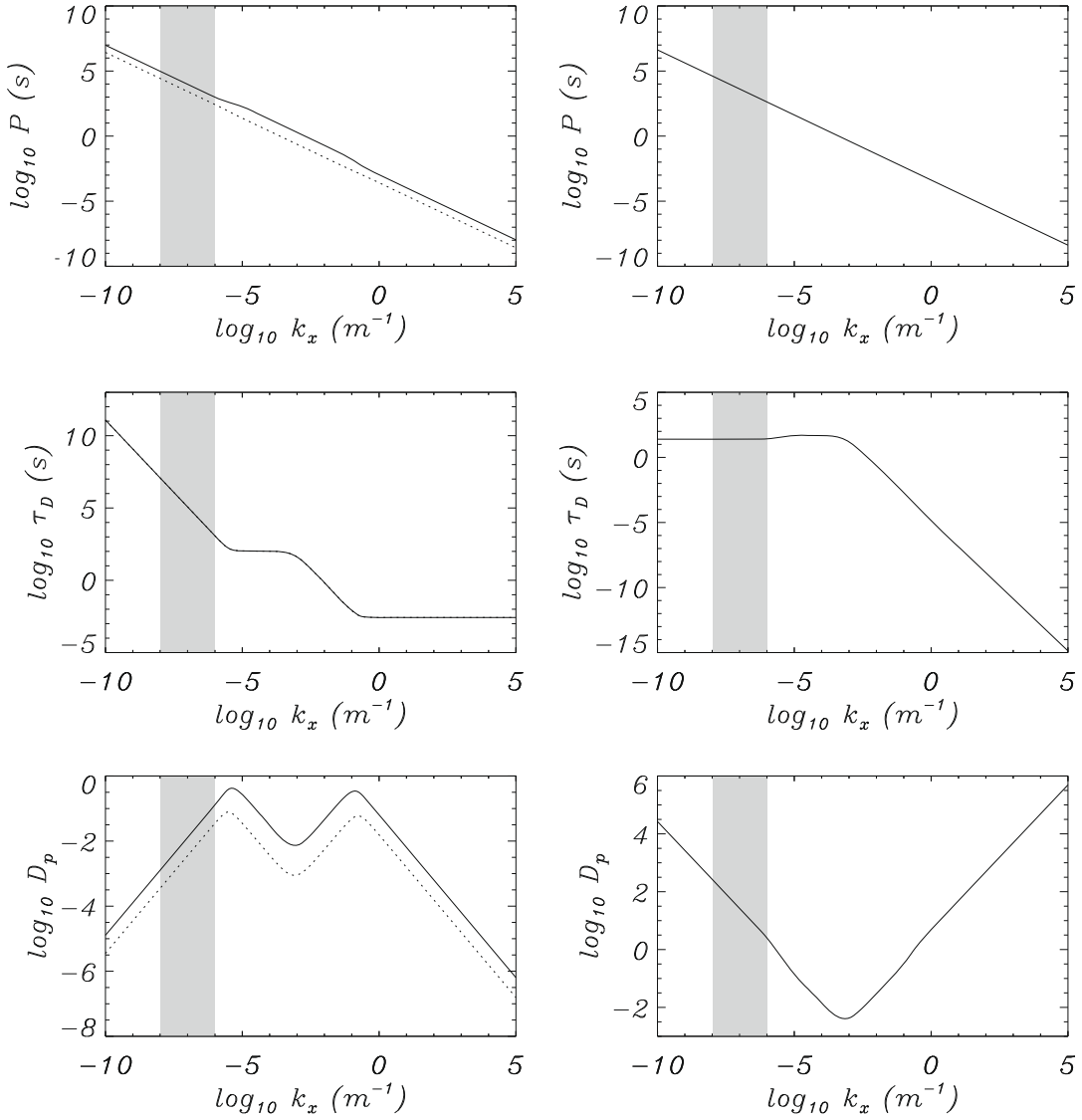

Fig. 3. Period (P), damping time (τ_D) and damping per period (D_p) versus the wavenumber, k_x, for the slow (left panels), and thermal (right panels) waves. The speed of the flow is $v_0 = 15$ km/s. The shaded regions indicate the interval of observed wavelengths.

focussed in the behaviour of slow and thermal waves by considering only field-aligned propagation. In this case, the fast wave becomes an Alfvén wave, propagating undamped, while slow and thermal waves remain coupled.

For our calculations we have considered the same values of the density, temperature and magnetic field and parameters corresponding to prominence regime 1.1 (Carbonell et al., 2004). Furthermore, previous calculations have also shown that the damping is independent of the heating mechanism considered, therefore, only a constant heating per unit volume has been considered. With these values, sound and Alfvén speeds in the prominence medium are 11.7 km/s and 126.1 km/s, respectively. Furthermore, the period of the waves is given by $P = \frac{2\pi}{\omega_R}$, the damping time is $\tau_D = \frac{1}{\omega_I}$ and the damping per period is $D_p = \frac{\omega_I}{\omega_R}$, all of them measured by an observer external to the flow.

Fig. 3 shows the results obtained for slow and thermal waves for a magnetic field-aligned flow having a typically observed constant speed v_0 of 15 km/s. In this case, the ordering of the characteristic speeds is $c_s < v_0 < c_a$, and this figure shows the unfolding of the period for the slow waves as well as the appearance of a finite period for the thermal wave, which becomes a propagating wave. Also, in the case of slow waves the unfolding of the period produces two different curves representing the damping per period, one shifted downwards and the other upwards and then, as a consequence, the slow wave having a higher period is more rapidly attenuated than the other one. On the other hand, due to the finite period of the thermal wave the damping per period of this wave becomes finite.

A careful look to Fig. 3 reveals that the high-period branch of the slow wave displays a bump in the wavenumber interval 10^{-6}–10^{-1} m^{-1} while in the low-period branch this feature cannot be seen. The period is computed from

$$P = \frac{2\pi}{k_x(v_0 \pm \Lambda_R)}, \tag{28}$$

having a very large interval of variation, which suggests that a logarithmic plot is the most convenient way to represent it. In Fig. 4, we display the behaviour of $(v_0 \pm \Lambda_R)$ versus $\log k_x$, which shows that two symmetric bumps appear for the mentioned wavenumber interval and that these features are due to the profile of the non-adiabatic sound speed. Then, when the logarithm of expression (28) is plotted versus the logarithm of the wavenumber, the above symmetry is broken and in one of the branches, corresponding to $(v_0 - \Lambda_R)$, the bump is clearly seen while in the other branch it is extremely difficult to observe it. In summary, a non-logarithmic plot of the period versus the wavenumber would show two symmetric bumps, in opposite directions because of the $\pm$ signs, caused by the profile of the non-adiabatic sound speed.

In Fig. 3, we observe that within the shaded interval the damping per period for the high-period branch of the slow wave varies between 10^{-3} and 10^{-1}, while for the thermal wave it varies between 10^3 and 1. Terradas et al. (2002) found that damping times were between two and three times the period, then, since $\tau_D = \frac{P}{2\pi D_p}$ we can impose these two limits and derive the value of D_p. The obtained values are $D_p = 8 \times 10^{-2}$–5×10^{-2}, which, within the range of observed wavelengths can be satisfied by the slow wave. On the contrary, these values of D_p cannot be fulfilled, within the wavenumber interval considered, by the thermal wave since it damps too quickly.

Next, for a fixed wavenumber, we have studied the effect of the flow speed on the wave periods and damping per period. We have

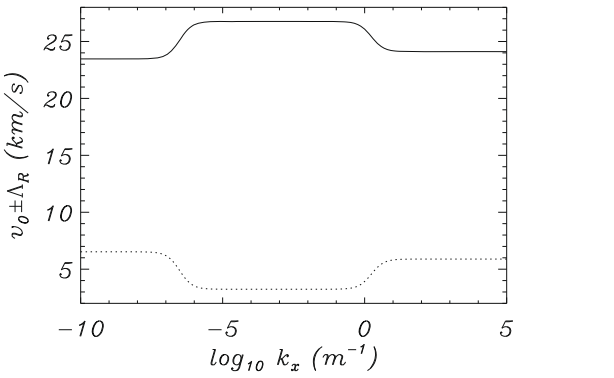

Fig. 4. Plot of the flow speed plus (continuous line)/minus (dashed line) the real part of the non-adiabatic sound speed, Λ_R, versus the wavenumber, k_x, for prominence regimes 1.1. The flow speed is $v_0 = 15$ km/s.

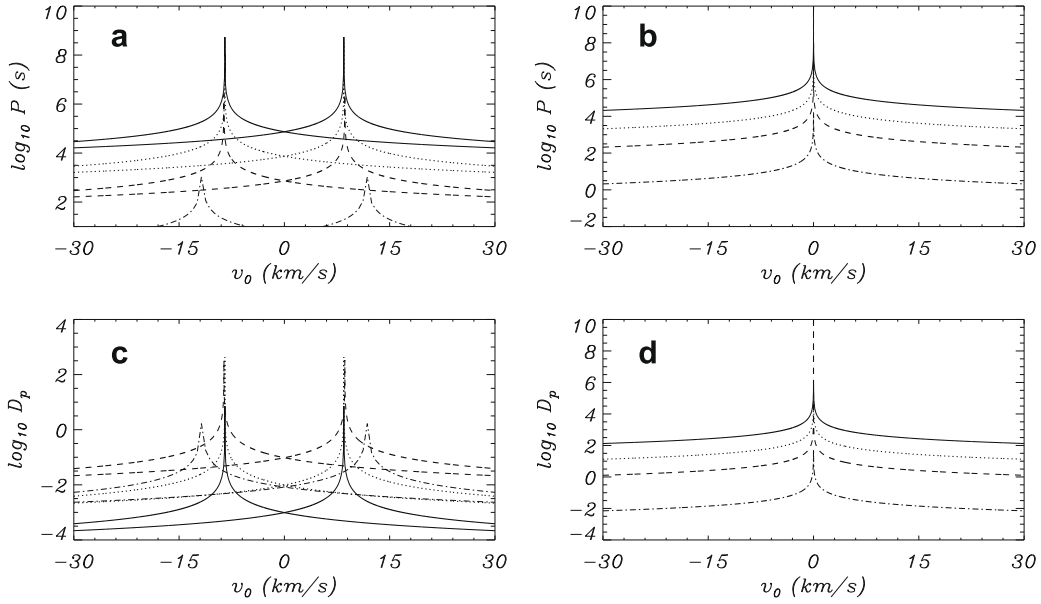

Fig. 5. (a, b) Period (P) and (c, d) damping per period (D_p) versus the flow speed, v_0, for the slow and thermal waves, respectively, for wavenumbers $k_x = 10^{-8}$ m^{-1} (continuous line), $k_x = 10^{-7}$ m^{-1} (dotted line), $k_x = 10^{-6}$ m^{-1} (dashed line) and $k_x = 10^{-4}$ m^{-1} (dashed-dotted line).

considered four different wavenumbers, $10^{-8}\,\mathrm{m}^{-1}$, $10^{-7}\,\mathrm{m}^{-1}$, $10^{-6}\,\mathrm{m}^{-1}$ and $10^{-4}\,\mathrm{m}^{-1}$, and a flow speed which varies between -30 km/s and +30 km/s covering the range of observed flow speeds. The results are shown in Fig. 5 and several features are of interest. First of all, the figure shows that for the thermal wave (panels b and d) the period and the damping per period become infinite in the case of no flow, and decrease with the flow strength and the wavenumber, as expected. In the case of slow waves (panels a and c), the behaviour is somewhat different since the period and the damping per period go to infinity for the same negative and positive flow speed whose absolute value matches the value of the real part of the non-adiabatic sound speed. This can be easily checked by computing Eq. (27) for physical conditions corresponding to prominence regime 1.1 and comparing the obtained values with the position of the peaks in Fig. 5, which points out that it is of capital interest to know the behaviour, with the wavenumber, of the real part of non-adiabatic sound speed. The figure also shows that the damping per period increases dramatically for positive or negative flow speeds close to the non-adiabatic sound speed and that, such as happens in the thermal wave, when the wavenumber is increased the periods of the slow waves decrease. Furthermore, in Fig. 5a it is clear that to the left of the peak located in the negative zone of flow speed both slow waves propagate in the direction of the negative x-axis (a backward wave appears), while between the peaks they propagate in opposite directions, and to the right of the peak located in the positive flow speed zone they propagate in the direction of the positive x-axis (a backward wave appears, again). Finally, for wavenumbers smaller than $10^{-4}\,\mathrm{m}^{-1}$, and once the wavenumber has been fixed, the period of the slow waves goes to infinity at different flow speeds when different prominence regimes are considered, and this occurs within the region of observationally determined wavelengths.

4. Observational implications

Considering the slow wave and taking P_0 as the period for the adiabatic case without flow, and P as the period for the adiabatic or non-adiabatic cases with flow, both periods are related by the expression:

$$\frac{P}{P_0}=\frac{c_s}{v_0\pm\Lambda_R}. \tag{29}$$

Then, for a fixed flow velocity and physical conditions, which determine the adiabatic sound speed, the ratio between periods depends on the behaviour of the real part of the non-adiabatic sound speed. The behaviour of the ratio P/P_0 versus the horizontal wavenumber, for a fixed flow velocity, can be seen in Fig. 6. Of course, in Fig. 6 the location of the curves corresponding to the cases with flow depends on the sign considered in Eq. (29), so, they are shifted downwards/upwards when the positive/negative sign is considered. In this figure, we can see the shift in period when flow is considered, but when only the flow is considered, and no other effects are taken into account, the period ratio is a constant. When only non-adiabatic effects are considered, the effect of the profile of the real part of the non-adiabatic sound speed is to increase the period ratio for some wavenumber intervals. When flow and non-adiabatic effects are considered together, the increase/decrease of the period ratio for some wavenumber intervals caused by non-adiabatic effects corresponds to the positive/negative sign in Eq. (29). This figure points out that when flow and non-adiabatic effects are considered, and depending on the wavenumber, the external observer can measure a period quite different from that of the wave in the flow's reference frame. In Fig. 7, the behaviour of the period ratio, corresponding to the non-adiabatic and adiabatic cases, versus the flow speed, and for a fixed wavenumber, is shown. It can be seen that the differences in the period ratio decrease as the flow speed is increased,

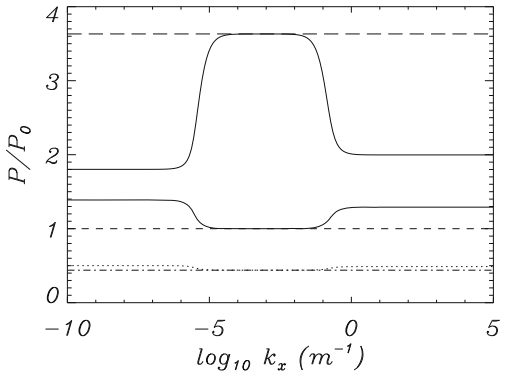

Fig. 6. Slow wave: ratio of P/P_0 versus the wavenumber, k_x. Adiabatic case without flow (short-dashed line); adiabatic case with flow considering positive sign in Eq. (29) (dotted-dashed line); Adiabatic case with flow considering the negative sign in Eq. (29) (long-dashed line); non-adiabatic case without flow (continuous line); non-adiabatic case with flow considering the positive sign in Eq. (29) (dotted line); non-adiabatic case with flow considering the negative sign in Eq. (29) (three-dotted-dashed line). The flow speed is $v_0 = 15$ km/s.

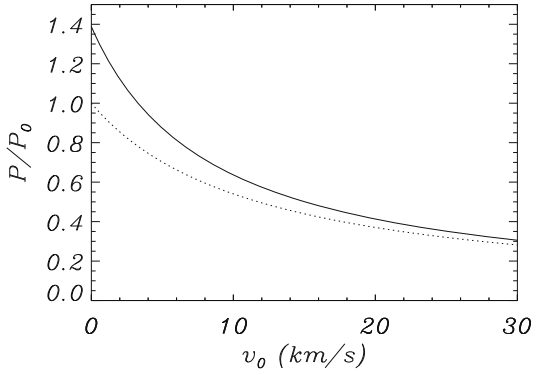

Fig. 7. Slow wave: ratio of P/P_0 versus the flow speed, v_0. Adiabatic case (dotted line); non-adiabatic case (continuous line). The fixed wavenumber is $k_x = 10^{-7}\,\mathrm{m}^{-1}$.

and the behaviour is exactly the same for any considered wavenumber.

On the other hand, a comparison between the periods and damping times for slow and thermal waves (Fig. 3) points out that these waves cannot have the same period or damping time for a fixed k_x. However, there is another possibility which cannot be ruled out. Imagine that two perturbations, with wavenumbers k_x and k'_x, excite thermal and slow waves whose real parts of the frequencies are given by

$$\omega_{\mathrm{slow}}=k_x(v_0\pm\Lambda_R),\quad \omega'_{\mathrm{slow}}=k'_x(v_0\pm\Lambda'_R),$$
$$\omega_{\mathrm{thermal}}=k_x v_0,\quad \omega'_{\mathrm{thermal}}=k'_x v_0$$

then

$$\frac{\omega_{\mathrm{slow}}}{\omega'_{\mathrm{thermal}}}=\frac{k_x(v_0\pm\Lambda_R)}{k'_x v_0}$$

and we can conclude that in order to have the same period or frequency the condition to satisfy is

$$k'_x=k_x\left(1\pm\frac{\Lambda_R}{v_0}\right). \tag{30}$$

This result points out that in the observer's rest frame one could not distinguish in terms of period between a slow and a thermal wave having different wavelengths which are related by the above expression. A similar condition can be found for the damping times, in this case we need to use an approximation to the imaginary part

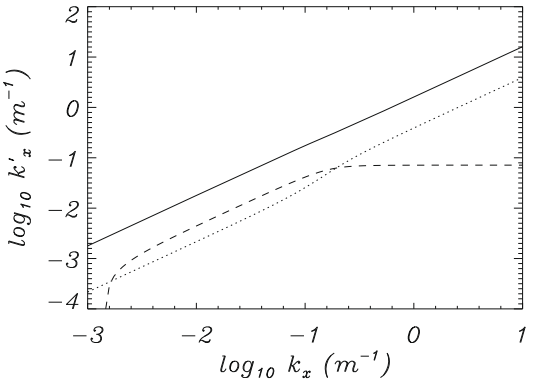

Fig. 8. Plot of k'_x, thermal wave wavenumber, versus the k_x, slow wave wavenumber, corresponding to Eq. (30) (solid and dotted lines) and (31) (dashed line). The flow speed is $v_0 = 15$ km/s.

of the frequency of the thermal wave which is given by $\omega^I_{\text{thermal}} \approx (\gamma-1)[k_\parallel k'_x + \rho_0 L_T]T_0/p_0$, while the imaginary part of the frequency of the slow wave is given by $\omega^I_{\text{slow}} = k_x \Lambda_I$, with Λ_I the imaginary part of the non-adiabatic sound speed. Now, imposing the equality of the damping times of both waves we obtain

$$k'_x \approx \left[\frac{p_0 k_x \Lambda_I}{(\gamma-1)T_0 k_\parallel} - \frac{\rho_0 L_T}{k_\parallel}\right]^{0.5}. \tag{31}$$

Thermal and slow waves whose wavenumbers are related by the above expression have the same damping times.

Now, we may wonder if there is any possibility that thermal and slow waves have the same period and the same damping time simultaneously, i.e. the same D_p. In order to check this possibility, we have plotted in Fig. 8 the wavenumber k'_x versus the wavenumber k_x, obtained from Eqs. (30) and (31) and we observe that the low frequency branch of the slow wave is intersected by the curve representing Eq. (31). Therefore, there are two pairs of (k_x, k'_x) for which the period and damping time of slow and thermal waves are equal. All this means that the knowledge of the wavelength and the flow speed becomes essential for a proper identification of involved waves, and that in presence of flow, the problem of wave identification becomes very complicate since, apart of fast waves which are not considered in this study, we can be confused,

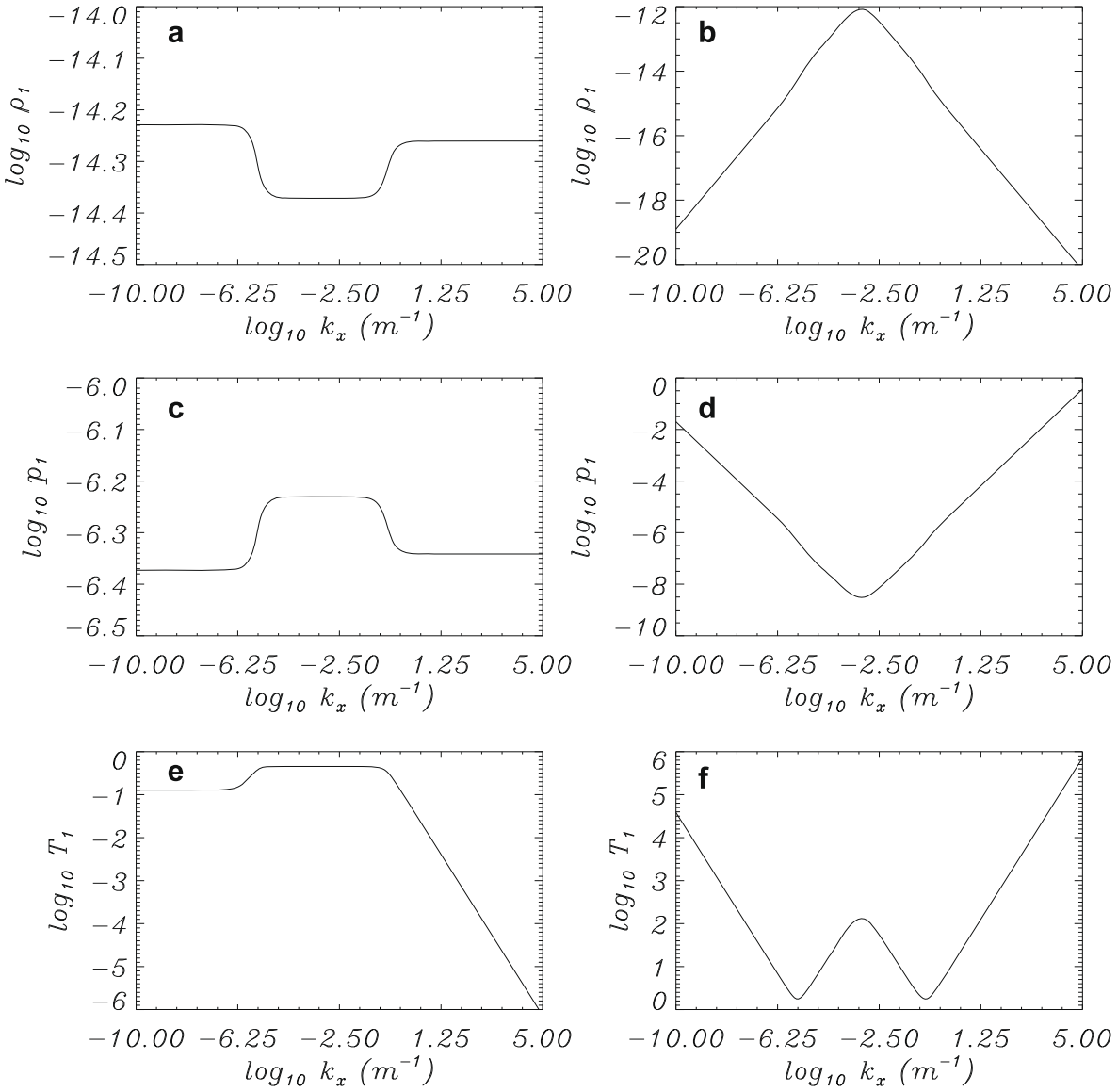

Fig. 9. Density (ρ_1), pressure (P_1) and temperature perturbations (T_1), in arbitrary units, versus the wavenumber, k_x corresponding to the slow wave (a,c,e), and the thermal wave (b,d,f). The flow speed is $v_0 = 15$ km/s.

in period and damping time, by the presence of propagating slow and thermal waves. It is also worth to mention that the equality of periods can be obtained in the whole range of considered wavenumbers while the equality of damping times or both damping times and periods can only be attained in a narrow interval of wavenumbers between 10^{-3} m^{-1} and 10^{-1} m^{-1}. Then, the remaining question now is: how could we distinguish between a slow and a thermal wave having the same period, the same damping time, or both? One possibility to consider is to look to the behaviour of pressure, density and temperature perturbations corresponding to slow and thermal waves. Fig. 9 shows that for slow and thermal waves density and pressure perturbations are very small. However, when the temperature perturbations of both waves are compared, the thermal wave temperature perturbation is much larger, for all the wavenumber interval considered, than the one corresponding to the slow wave. Then, if we could obtain any information about temperature perturbations in prominence oscillations driven by MHD non-adiabatic waves with flow, a difficult task, this information could help us to discriminate between the slow and thermal waves involved in the oscillations.

5. Conclusions

Taking into account that the observations of small-amplitude oscillations in prominences/filaments report that they are damped in time and, also, that material flows are a common feature, our main aim in this paper has been to analyse the effect of a field-aligned background flow on the damping of non-adiabatic MHD waves potentially responsible for the time damped oscillations in prominences/filaments and to point out the important role played by the non-adiabatic sound speed. Furthermore, we have also highlighted some observational consequences, because of the presence of flow, which can difficult a proper identification of waves involved in the oscillations. Since non-adiabatic effects do not contribute in a significant way to the damping of fast waves, we have focussed on the time damping of slow and thermal waves by considering only field-aligned propagation. Our results point out that in the case of slow waves, and for any horizontal wavenumber, the greatest finite damping per period is obtained for values of the flow speed close to the non-adiabatic sound speed of the prominence medium. In the case of the thermal wave, and for any horizontal wavenumber, an infinite damping per period is obtained when no flow is present, becoming finite as soon as a flow is considered. The finite period and damping per period obtained for the thermal wave suggest that, when flows and time damped oscillations are observed in a prominence/filament, this wave should be also taken into account as potentially responsible of the observed damped oscillations. We have also found that there is the possibility that slow and thermal waves, having different wavelengths, may have the same period, the same damping time, or both simultaneously, which could lead to a wrong identification of the waves involved in the oscillations. One possibility to discriminate is to resort to density, pressure and temperature perturbations, since, these perturbations, or at least the temperature perturbation, should produce a clear observational feature which should help to perform the discrimination. Then, if flows are ubiquitous features in prominences/filaments the observationally determined periods and damping per period include this effect, therefore, theoretical models must include this feature in order to perform meaningful comparisons with observations.

On the other hand, an interesting feature mentioned in observations is counterstreaming, simultaneous flowing in opposite direction in adjacent prominence/filament threads. Considering this case and assuming flows with the same speed but opposite direction in adjacent media a few qualitative conclusions could be put forward. If the flow speed is greater than the sound speed, in one medium all the waves, slow and thermal, propagate towards the right while in the other medium they will propagate towards the left. When the flow speed is smaller than the sound speed, in one medium the thermal wave and one of the slow waves propagate towards the right while the other slow wave propagates towards the left, although in the other medium the situation is reversed. The situations described before point out that we need a very high-spatial resolution in our observations in order not to get a zero signal as a net result. This zero signal would be due to the cancelling of signals coming from waves propagating in different directions, with the same phase speed and amplitude, in adjacent threads. On the contrary, an enhanced signal could be also obtained due to the superposition of signals coming from waves propagating with the same phase speed and in the same direction but within different threads. Finally, the third situation corresponds to the case in which the flow speed matches exactly the sound speed, then, in both media we will have a thermal and a slow wave propagating, in one case, towards the right while in the other they propagate towards the left. In this case, signals coming from the slow and thermal waves could again cancel without a good spatial resolution. Summarizing, poor spatial resolution observations of prominence threads, in which flows and oscillations are present, would produce a mixture of oscillatory signals. The mixed oscillatory signal, coming from different waves propagating in different directions in adjacent threads, would be misleading giving erroneous information about wave properties and character. Furthermore, if non-adiabatic effects are taken into account the situation worsens, since the non-adiabatic sound speed is not constant and depends on the wavenumber.

The study and understanding of prominence/filaments oscillations is a challenging task from the observational and theoretical point of view. The number of different physical effects (non-adiabaticity, flows, partial ionization, etc.) involved suggests that they must be explored in a systematic manner in order to obtain a full understanding of the properties of these oscillations.

Acknowledgements

The authors acknowledge the financial support received from Ministerio de Educación y Ciencia under grant AYA2006-07637, and from the Government of the Balearic Islands under grant PCTIB2005GC3-03. J.L.B. wants to acknowledge the ISSI team on Spectroscopy and Imaging of Quiescent and Eruptive Solar Prominences from Space, for useful interactions.

References

Ballester, J.L., 2006. Proc. Phil. Trans. Roy. Soc. A 364, 405.
Banerjee, D., Erdélyi, R., Oliver, R., O'Shea, E., 2007. Solar Phys. 246, 3.
Carbonell, M., Oliver, R., Ballester, J.L., 2004. A&A 415, 739.
Dahlburg, R.B., Mariska, J.T., 1988. Solar Phys. 117, 51.
Goedbloed, H., Poedts, S., 2004. Principles of Magnetohydrodynamics. Cambridge University Press.
Hildner, E., 1974. Solar Phys. 35, 123.
Lin, Y., Engvold, O., Wiik, J.E., 2003. Solar Phys. 216, 109.
Lin, Y., 2004. Ph.D. Thesis. University of Oslo, Norway.
Lin, Y., Engvold, O., Rouppe Van der Voort, L.H.M., Van Noort, M., 2007. Solar Phys. 246, 65.
Milne, A.M., Priest, E.R., Roberts, B., 1979. ApJ 232, 304.
Molowny-Horas, R., Oliver, R., Ballester, J.L., Baudin, F., 1997. Solar Phys. 172, 181.
Molowny-Horas, R., Wiehr, E., Balthasar, H., Oliver, R., Ballester, J.L., 1999. In: Antalová, A., Balthasar, H., Kucera, A. (Eds.), JOSO Annual Report 1998. Astronomical Institute Tatranská Lomnica, p. 126.
Oliver, R.J., Ballester, J.L., 2002. Solar Phys. 206, 45.
Rosner, R., Tucker, W.H., Vaiana, G.S., 1978. ApJ 220, 643.
Terradas, J., Oliver, R., Ballester, J.L., 2001. A&A 378, 635.
Terradas, J., Molowny-Horas, R., Wiehr, E., Balthasar, H., Oliver, R., Ballester, J.L., 2002. A&A 393, 637.
Terradas, J., Carbonell, M., Oliver, R., Ballester, J.L., 2005. A&A 434, 741.
Soler, R., Oliver, R., Ballester, J.L., 2007. A&A 471, 1023.
Zirker, J.B., Engvold, O., Martin, S.F., 1998. Nature 396, 440.